PAPER

Check for updates

Explorations of highly birefringent materials in the vanadium oxyfluoride–iodate system by fluoride ion modulation†

Yu Huang,[ab] Xue-Ying Zhang,[a] San-Gen Zhao, [a] Jiang-Gao Mao [ac] and Bing-Ping Yang [ac]

Birefringent materials are of great interest because of their ability to manipulate light. The demand for smaller devices has driven the development of new birefringent materials with high levels of birefringences and overall excellent physicochemical properties. Two such materials, $Sr[VO_2F(IO_3)_2]$ and $Sr_3F_2(VO_2F_4)(IO_3)$, have been successfully synthesized by exploring the VOF polyhedron–iodate system. The compounds exhibit remarkable birefringence values of 0.250 and 0.406 at 550 nm, respectively, which are significantly higher than those of the commercially available birefringent vanadate (YVO_4, 0.204 at 532 nm), and the compound $Sr_3F_2(VO_2F_4)(IO_3)$ has the largest birefringence in the iodate-fluoride system. $Sr[VO_2F(IO_3)_2]$ is composed of polymerized anionic groups, $[VO_2F(IO_3)_2]^{2-}$, while $Sr_3F_2(VO_2F_4)(IO_3)$ is composed of optimally arranged IO_3^- and fluorinated $VO_2F_4^{3-}$ functional groups organized by the $Sr_3F_2^{4+}$ positively charged structure-oriented templates. The compounds have a wide optical transmission range of 0.28–10.7 μm and 0.43–10.3 μm, respectively. Moreover, they exhibit high thermal stability with values of 366 and 319 °C, respectively. These properties make them suitable for use in the middle-wavelength infrared region. The study demonstrates that hybridizing anionic functional groups and modulating the structure with anions are effective crystal engineering strategies for developing high-performance inorganic optical materials.

Introduction

Linear optical birefringent crystals are of interest because of their ability to split a ray of light into two perpendicularly polarized components.[1,2] They are critical components of devices such as polarimeters, fiber-optic isolators, and circulators.[3–5] Some commonly used birefringent crystals include α-BaB_2O_4 (0.122 at 532 nm),[6] $CaCO_3$ (0.172 at 532 nm),[7] TiO_2 (0.256 at 546 nm),[8] YVO_4 (0.204 at 532 nm),[9] and $LiNbO_3$ (0.0738 at 1440 nm).[10,11] While natural birefringent crystals such as $CaCO_3$ and TiO_2 often have geological impurities or mechanical processing problems,

and α-BaB_2O_4 and $LiNbO_3$ have relatively low birefringence (Δn), vanadate YVO_4 crystals have been widely used as birefringent materials owing to their high birefringences and excellent machinability.[9] The development of new birefringent materials with remarkable properties and excellent overall performance has been driven by the need for device miniaturization.[12–14]

The relationship between the optical properties of materials and their structures is significant. Therefore, materials with high birefringences can be designed by utilizing microscopic anisotropic functional units.[15–17] Inorganic compounds show promise due to their optical transmission, mechanical processing, and physicochemical properties. Inorganic anisotropic units can be classified into three categories: (1) cations with stereochemically active lone electron pairs (SCALP) (such as Sn^{2+}, Pb^{2+}, and Sb^{3+}),[18–21] (2) transition-metal polyhedra with second-order Jahn–Teller (SOJT) distortions (such as V^{5+} and Nb^{5+}),[22] and (3) planar π-conjugated anions (such as BO_3^{3-}, NO_3^-, and CO_3^{2-}).[23–26] Conventional birefringent materials consist of the latter two types of anisotropic units; however, compounds with SCALP have only recently been discovered as birefringent materials, such as SnF_2 (Δn, 0.191 at 546 nm)[27] and $BaSn_2(PO_4)_2$.[28] I^{5+} containing iodates typically have high birefringences and are emerging as a promising class of birefringent materials.[29–33]

a State Key Laboratory of Structural Chemistry, Fujian Institute of Research on the Structure of Matter, Chinese Academy of Sciences, Fuzhou, 350002, Fujian, China. E-mail: ybp@fjirsm.ac.cn
b State Key Laboratory of Material Processing and Die & Mould Technology, School of Materials Science and Engineering, Huazhong University of Science and Technology, Wuhan, 430074, Hubei, China
c University of Chinese Academy of Sciences, Beijing, 100049, China

† Electronic supplementary information (ESI) available: Supporting Information is available and includes additional crystallographic data and local dipole moments (Tables S1–S5), Fig. S1–S11, and cif files of crystal structures. CCDC 2299803 and 2299804. For ESI and crystallographic data in CIF or other electronic format see DOI: https://doi.org/10.1039/d4tc01200c

7286 | *J. Mater. Chem. C,* 2024, **12**, 7286–7294

This journal is © The Royal Society of Chemistry 2024

The combination of two types of functional groups has proven to be a successful approach to study novel materials that benefit from the advantages of both groups. Such compounds include $Pb_2VO_2F_5$[18] and $M(IO_3)_2(NO_3)$ (M = Sc, In), etc.[34,35] In our previous work, $Pb_2(IO_3)(PO_4)$,[36] an iodate–phosphate with improved birefringence and preserved band gap, was successfully synthesized by incorporating IO_3^- groups into phosphates. Fluorine element is considered effective for broadening the optical transmission range and forming structure-oriented templates because it has the highest electronegativity and multiple bridging modes. By introducing iodates into hafnium fluorides, we have synthesized a birefringent material, $HfF_2(IO_3)_2$. This material exhibits a large birefringence of 0.333 at 550 nm and a wide band gap of 4.11 eV, combining the advantages of iodates and fluorides.[37]

We explored new birefringent materials in the VOF polyhedron–iodate system to enhance the properties of vanadate YVO_4. Two new birefringent materials were successfully synthesized: $Sr[VO_2F(IO_3)_2]$ with polymerized anionic groups and $Sr_3F_2(VO_2F_4)(IO_3)$ with discrete IO_3^- and fluorinated $VO_2F_4^{3-}$ functional groups. The structure was modulated by adjusting the fluorine content. $Sr_3F_2(VO_2F_4)(IO_3)$ displays an ultrahigh birefringence of 0.406 at 550 nm, which is the largest in the iodate-fluoride system and has a wide transmittance range of 0.43 to 10.3 μm. Additionally, it remains stable at temperatures up to 319 °C. This paper presents the synthesis, structural analysis, optical characterization, and theoretical calculations of both compounds.

Experimental methods

Synthesis of $Sr[VO_2F(IO_3)_2]$ and $Sr_3F_2(VO_2F_4)(IO_3)$

$Sr[VO_2F(IO_3)_2]$ and $Sr_3F_2(VO_2F_4)(IO_3)$ were synthesized using a conventional hydrothermal method. The starting materials for $Sr[VO_2F(IO_3)_2]$ were SrO (0.0518 g, 0.5 mmol), V_2O_5 (0.3638 g, 2 mmol), HIO_3 (0.7036 g, 4 mmol), HF (0.5 mL), and H_2O (2 mL). The mixture was placed in a Teflon liner (23 mL), sealed in a stainless steel autoclave, heated at 200 °C for 72 hours, and cooled to 35 °C at a rate of 3 °C h^{-1}. Pale yellow crystals of $Sr[VO_2F(IO_3)_2]$ were obtained with a yield of 50% (based on Sr) after washing and drying. $Sr[VO_2F(IO_3)_2]$ is iso-structural to α-$Ba[VO_2F(IO_3)_2]$ previously reported by Hongwei Yu et al. The synthesis of $Sr[VO_2F(IO_3)_2]$ required more HIO_3 and lower temperatures than the synthesis of α-$Ba[VO_2F(IO_3)_2]$ (220 °C).[38] $Sr_3F_2(VO_2F_4)(IO_3)$ was synthesized using SrO (0.0518 g, 0.5 mmol), V_2O_5 (0.0909 g, 0.5 mmol), HIO_3 (0.1759 g, 1 mmol), HF (0.5 mL), and H_2O (2 mL) at a reaction temperature of 230 °C. Yellow flake crystals of $Sr_3F_2(VO_2F_4)(IO_3)$ were obtained in a higher yield (60%, based on Sr).

The molar ratios of the F, V, and I elements in the reactants play a critical role in synthesizing $Sr[VO_2F(IO_3)_2]$ and $Sr_3F_2(VO_2F_4)(IO_3)$. The former requires a low F : V : I molar ratio of about 3 : 1 : 1, while the latter requires a much higher F : V : I molar ratio of about 11 : 1 : 1. Temperature also affects the formation of these compounds, with $Sr[VO_2F(IO_3)_2]$ crystallizing at around 200 °C and $Sr_3F_2(VO_2F_4)(IO_3)$ forming at a higher temperature of 230 °C.

Single crystal X-ray diffraction

Single crystal X-ray diffraction data for the two compounds were collected at 295 K using an Agilent SuperNova dual-wavelength CCD diffractometer with Mo Kα radiation (λ = 0.71073 Å). The data were reduced using the CrysAlisPro software package. Numerical absorption corrections were applied using Gaussian integration over a multifaceted crystal model, along with empirical absorption corrections using spherical harmonics implemented in the SCALE3 ABSPACK scaling algorithm.[39] The structures were determined using the direct method and refined through full-matrix least-squares fitting on F^2 with SHELXL-2017.[40] All atoms were refined with anisotropic thermal parameters. The crystal structures were examined for missing symmetry elements using PLATON, and no such elements were found.[41] Crystallographic data and information on structure refinement can be found in Table S1 (ESI†), while selected bond lengths and angles are presented in Tables S2 and S3 (ESI†). Detailed information on the crystal structure of the two compounds (CCDC 2299803 and 2299804).†

Powder X-ray diffraction

Powder X-ray diffraction (PXRD) data were collected using a Rigaku MiniFlex600 diffractometer equipped with Cu Kα radiation (λ = 1.5418 Å) over a 2θ range of 10–70° with a scan step width of 0.02°.

Energy-dispersive X-ray spectroscopy

Compositional elemental analyses were performed using a field emission scanning electron microscope (JSM6700F) equipped with an Oxford INCA energy dispersive X-ray spectroscope.

Infrared spectroscopy

Infrared (IR) spectra were measured using a Nicolet Magna 750 Fourier transform infrared spectrometer in the 4000–400 cm^{-1} spectral region. The samples were prepared as pellets with KBr powder.

Ultraviolet-visible-near-IR diffuse reflectance spectra

Ultraviolet-visible-near-IR (UV-vis-NIR) diffuse reflectance spectra were collected using a PerkinElmer Lambda 950 UV-vis-NIR spectrophotometer. A $BaSO_4$ powder plate served as a 100% reflectance reference. The diffuse reflectance data were converted to absorption data using the Kubelka–Munk function $\alpha/S = (1 - R)^2/2R$, where α is the absorption coefficient, S is the scattering coefficient, and R is the reflectance.[42] The band gap values were extrapolated from the absorption edge to zero absorption in the plots of α/S versus energy.

Thermal analysis

A NETZCH STA 449F3 thermal analyzer was used to perform thermogravimetric analysis (TGA) and differential scanning calorimetry (DSC). The measurements were carried out between 30 and 1000 °C at a heating rate of 10 °C min^{-1} under a flowing

This journal is © The Royal Society of Chemistry 2024

J. Mater. Chem. C, 2024, 12, 7286–7294 | 7287

N_2 atmosphere. An Al_2O_3 crucible was used as the sample container, and an empty crucible was used as the reference.

Birefringence measurements

The birefringence of the sample was measured using a polarizing microscope (NIKON ECLIPSE LV100N POL) equipped with a Berek compensator at a wavelength of 550 nm. The retardation (Γ) can be calculated using the formula $\Gamma = |n_e - n_o| T = \Delta nT$, where Δn is the birefringence and T is the crystal thickness. The retardation can be determined by rotating the compensator positively and negatively.

Computational methods

The electronic and optical properties of the materials were calculated using the CASTEP code and the density functional theory (DFT) with the plane-wave pseudopotential method.[43,44] The generalized gradient approximation Perdew–Burke–Ernzerhof (PBE) exchange–correlation functional was utilized. The core-electron interactions were described using the norm-conserving pseudopotential.[45] The valence electron configurations of the atoms are Sr $5s^2$ $4p^6$ $3d^{10}$, V $3d^3$ $4s^2$, I $5s^2$ $5p^5$, O $2s^2$ $2p^4$, and F $2s^2$ $2p^5$. The number of plane-wave basis sets was determined using a cutoff energy of 850 eV. The Brillouin zone was sampled using the Monkhorst–Pack method with k-point sampling grids of $5 \times 2 \times 2$ and $1 \times 5 \times 2$ for $Sr[VO_2F(IO_3)_2]$ and $Sr_3F_2(VO_2F_4)(IO_3)$, respectively. The default values of the CASTEP code were used for other parameters and convergence criteria.

Results and discussion

Crystal structure

$Sr[VO_2F(IO_3)_2]$ crystallizes in the *Pbcn* (No. 60) space group. Its asymmetric unit contains one Sr, one V, one I, one F, and four O atoms. The structure of $Sr[VO_2F(IO_3)_2]$ consists of $[VO_2F(IO_3)_2]^{2-}$ polyanions and Sr^{2+} cations. Each I^{5+} cation is coordinated by three O^{2-} anions in a trigonal pyramidal geometry. The bond lengths between I and O are within the typical range of 1.799(8) to 1.850(7) Å for metal iodates.[46,47] Each V^{5+} cation is observed as a dioxovanadium(V) ion (VO_2^+) with V–O bond lengths of 1.621(7) Å. Each VO_2^+ ion is connected to a terminal F^- anion and two IO_3^- groups, forming a $[VO_2F(IO_3)_2]^{2-}$ polyanion (Fig. 1). The V–O bond lengths range from 1.621(7) to 1.968(7) Å, and the V–F bond length is 1.907(9) Å. The angle between the lone electron pairs of the two iodate groups is 12.06°, and the angle between the lone electron pairs and the a axis is 19.36°, caused by the presence of the V–O–I bridges. The $[VO_2F(IO_3)_2]^{2-}$ polyanions are arranged in parallel along the b axis. The polyanions $[VO_2F(IO_3)_2]^{2-}$ are separated by Sr^{2+} cations, which are connected to them by eight Sr–O and two Sr–F ionic bonds. The bond lengths range from 2.602(8) to 2.819(7) Å (See Fig. S1, ESI†). The bond valence sums of Sr (1.879), V (5.132), I (4.975), F (0.880), and O (1.854–2.299) are reasonable.[48,49]

In the structure of iso-structural α-$Ba[VO_2F(IO_3)_2]$,[38] the angle between the lone electron pairs of the two iodate groups is 10.96°, and the angle between the lone electron pairs and the
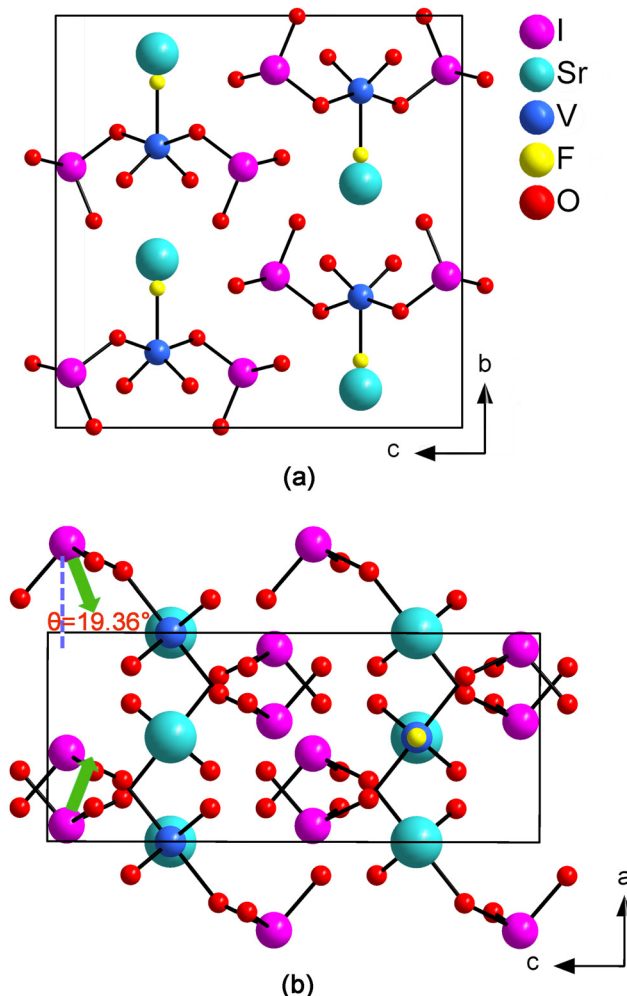
Fig. 1 View of the three-dimensional structure of $Sr[VO_2F(IO_3)_2]$ along the a axis (a) and along the b axis (b).

a axis is 18.76°. Because the Ba^{2+} ion has a larger radius than the Sr^{2+} ion, these angles in α-$Ba[VO_2F(IO_3)_2]$ are smaller than those in $Sr[VO_2F(IO_3)_2]$.

$Sr_3F_2(VO_2F_4)(IO_3)$ crystallizes in the $C2/c$ space group (No. 15). The asymmetric unit contains three Sr, one V, one I, six F, and five O atoms, all of which are in general positions. The $Sr_3F_2(VO_2F_4)(IO_3)$ compound contains V^{5+} cations that exist as dioxovanadium(V) cations (VO_2^+). However, unlike in $Sr[VO_2F(IO_3)_2]$, each VO_2^+ is bonded to four F^- anions, forming an octahedrally coordinated and discrete $VO_2F_4^{3-}$ complex anion (Fig. 2). The $VO_2F_4^{3-}$ octahedron has two short V–O vanadyl bonds of 1.603(8) and 1.692(6) Å and four V–F bonds ranging from 1.898(5) to 2.177(6) Å. This results in a strongly off-center distortion towards the specific O–O edge ($\Delta d = 0.95$), which is much larger than that of the NbO_6^{7-} octahedron ($\Delta d = 0.69$) of the $LiNbO_3$ birefringent crystal. Each I^{5+} cation is surrounded by three O^{2-} anions in a typical trigonal pyramidal geometry with normal I–O bond lengths ranging from 1.794(7) to 1.804(6) Å. In comparison to the $[VO_2F(IO_3)_2]^{2-}$ polyanion present in $Sr[VO_2F(IO_3)_2]$, the $VO_2F_4^{3-}$ complex anions with multiple fluorine atoms are positioned separately from the IO_3^-
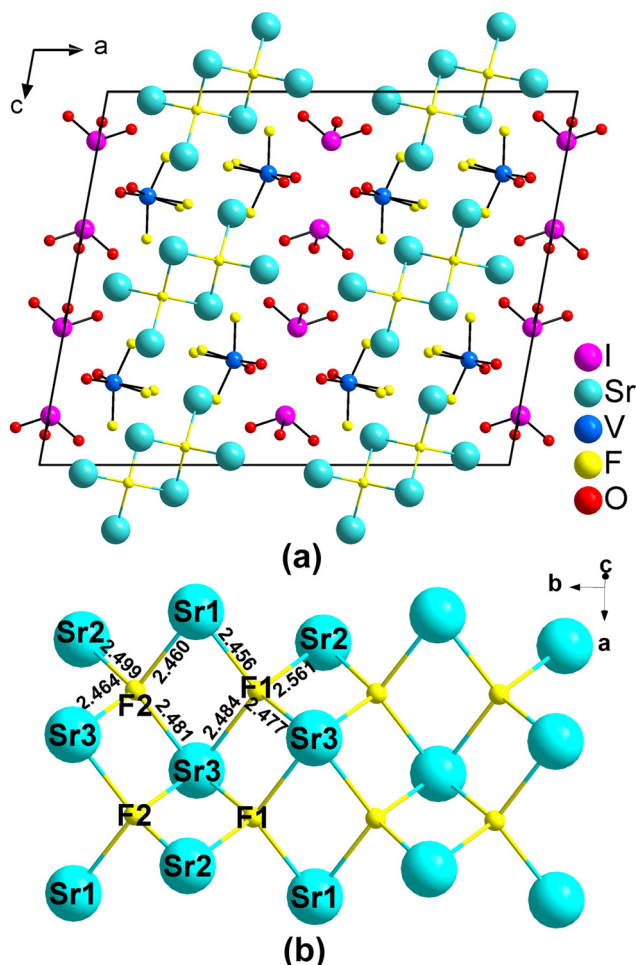
7288 | *J. Mater. Chem. C*, 2024, **12**, 7286–7294

This journal is © The Royal Society of Chemistry 2024

Fig. 2 Three-dimensional structure of $Sr_3F_2(VO_2F_4)(IO_3)$ viewed along the b axis (a). Diagram of the $_\infty[Sr_3F_2]^{4+}$ chain (b).

groups. This separation eliminates the V–O–I bridge bonds and allows for alignment of the $VO_2F_4^{3-}$ and IO_3^- groups along the c axis. The lone electron pairs of the iodate groups are arranged in a straight line, forming an angle of only 3.0° with the c axis. This angle is significantly smaller than the corresponding angles observed in $Sr[VO_2F(IO_3)_2]$.

Each F1$^-$ or F2$^-$ ion forms ionic bonds with four Sr^{2+} cations in the tetrahedral geometry, forming a chain of positively charged $Sr_3F_2^{4+}$ units. The Sr1^{2+}, Sr2^{2+} and Sr3^{2+} cations form ionic bonds with O^{2-} and F$^-$ ions of the $VO_2F_4^{3-}$ and IO_3^- groups (Fig. 2), serving as templates for the arrangement of the anionic functional units. The Sr–O bond lengths are 2.581(8)– 2.637(6), 2.666(7)–2.882(8), and 2.735(7) Å, respectively; the Sr–F bond lengths are 2.457(6)–2.573(5), 2.425(6)–2.876(6), and 2.464(5)–2.622(6) Å, respectively. The bond valence sums of Sr, I, V, F, and O are 2.054–2.166, 5.202, 4.901, 1.004–1.164, and 1.477–2.272, respectively. These values are consistent with their corresponding atomic valences.[48,49]

Thermal analysis

TGA and DSC curves show that $Sr[VO_2F(IO_3)_2]$ is stable at temperatures up to 366 °C (See Fig. S3, ESI†). Each molecule

then releases 1 I$_2$ molecule, 2.25 O$_2$ molecules, and 0.5 F$_2$ molecules. The calculated total mass loss (65.4%) is in agreement with the experimental value (65.2%). The TGA plot for $Sr_3F_2(VO_2F_4)(IO_3)$ in Fig. 3 shows a dramatic weight loss between 319 and 500 °C, followed by a small weight loss up to 1000 °C. The calculated mass loss of 0.5 I$_2$ molecules and 2.5 F$_2$ molecules released per formula unit (35.0%) is higher than the experimental value (30.1%), which is consistent with the continued loss of F$_2$ molecules above 1000 °C if the residue is assumed to be a mixture of $Sr_2V_2O_7$, SrO, and SrF$_2$.

Spectroscopic properties

Since the two compounds have identical chemical compositions, their optical spectra are similar. The IR spectra show high transparency in the 4000–1000 cm^{-1} (2.5–10 μm) region for both compounds (See Fig. S4, ESI†). For $Sr[VO_2F(IO_3)_2]$, the absorption bands at 970 and 906 cm^{-1} are attributed to V–O vibrations, while the other bands between 794 and 461 cm^{-1} are attributed to I–O vibrations. For $Sr_3F_2(VO_2F_4)(IO_3)$, the absorption peaks at 970–861 cm^{-1} and 807–418 cm^{-1} are assigned to the characteristic vibrations of V–O and I–O, respectively.

The UV-vis-NIR diffuse reflectance spectra indicate that $Sr[VO_2F(IO_3)_2]$ and $Sr_3F_2(VO_2F_4)(IO_3)$ have absorption cutoff edges at 285 and 431 nm, respectively (See Fig. S6, ESI†). The energy band gaps of $Sr[VO_2F(IO_3)_2]$ and $Sr_3F_2(VO_2F_4)(IO_3)$ are 2.39 and 2.33 eV, respectively, based on the extrapolation of the absorption edge to the baseline. The UV-vis-NIR and IR spectra indicate that $Sr[VO_2F(IO_3)_2]$ and $Sr_3F_2(VO_2F_4)(IO_3)$ (Fig. 4) possess a broad optical transmission range of 0.28–10.7 μm and 0.43–10.3 μm, respectively.

Birefringence properties

The birefringence of a single crystal of $Sr_3F_2(VO_2F_4)(IO_3)$ was measured using a polarizing microscope with a Berek compensator (Fig. 5). The measurements revealed a retardation (Γ) value of 1.815 μm and a crystal thickness (T) of 6.6 μm. By
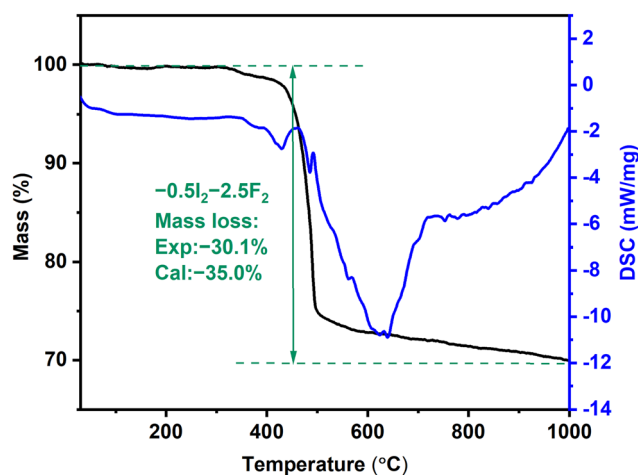

Fig. 3 TGA and DSC curves of $Sr_3F_2(VO_2F_4)(IO_3)$ under a N$_2$ atmosphere.

This journal is © The Royal Society of Chemistry 2024

J. Mater. Chem. C, 2024, **12**, 7286–7294 | **7289**

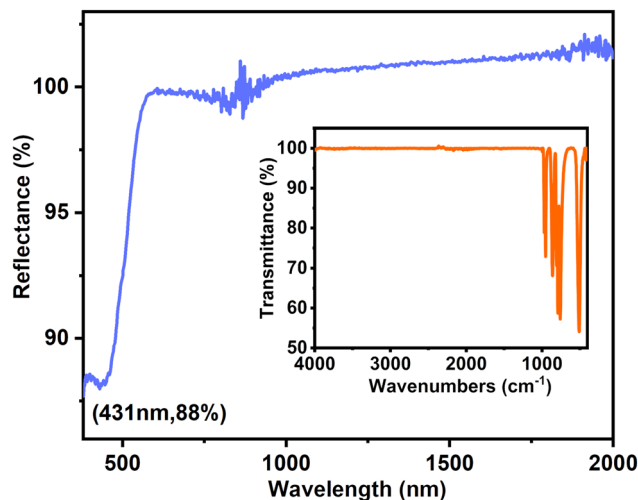**Fig. 4** UV-vis-NIR diffuse reflectance spectrum and IR spectrum (inset) of $Sr_3F_2(VO_2F_4)(IO_3)$.

applying the formula ($\Gamma = \Delta nT$), the birefringence of $Sr_3F_2(VO_2F_4)(IO_3)$ was measured to be 0.275 at a wavelength of 550 nm.

Theoretical calculation

To analyze the correlation between the optical properties and electronic structures of both compounds, we conducted DFT calculations. The band gaps of $Sr[VO_2F(IO_3)_2]$ and $Sr_3F_2(VO_2F_4)(IO_3)$ were theoretically calculated to be 2.88 and 2.66 eV, respectively, as shown in Fig. S7 (ESI†). The discrepancy between the theoretical and experimental values is due to the inherent limitations of the DFT method.

The optical properties of a material are generally related to the electronic states near the Fermi level. In the case of $Sr[VO_2F(IO_3)_2]$ and $Sr_3F_2(VO_2F_4)(IO_3)$, the distributions of the total and partial density of states are very similar, as shown in Fig. S8 (ESI†). The valence band is mainly occupied by O 2p and a small amount of I 5s and I 5p nonbonding electronic states, while the conduction band is dominated by unoccupied V 3d, O 2p, and I 2p orbitals. The band gap and optical properties of both compounds are determined by the interactions between I and O and between V and O.[50]

The linear refractive index is calculated as $n^2(\omega) = \varepsilon(\omega)$, while the complex dielectric function is expressed as $\varepsilon(\omega) = \varepsilon_1(\omega) + i\varepsilon_2(\omega)$. The equation below provides the imaginary component

(ε_2) of the dielectric function:[16]

$$\varepsilon_2^{ij}(\omega) = \frac{8\pi^2\hbar^2 e^2}{m^2 V}\sum_k \sum_{cv}(f_c$$
$$-f_v)\frac{p_{cv}^i(k)p_{vc}^j(k)}{E_{vc}^2}\delta[E_c(k) - E_v(k) - \hbar\omega] \quad (1)$$

The fundamental physical constants $\hbar$, e, m, and V represent Planck's constant, charge, electron mass, and unit cell volume, respectively. The Fermi–Dirac distribution functions for the conduction and valence bands are denoted by f_c and f_v, respectively. The term $p_{cv}^i(k)$ refers to the momentum matrix element transition between the conduction band (c) and valence band (v) energy levels at a specific k point in the Brillouin zones. The real part of the dielectric function is obtained by performing the Kramers–Kronig transformation.[51]

The calculations show that both compounds exhibit significant optical anisotropy and are optically negative biaxial crystals. At 550 nm, $Sr[VO_2F(IO_3)_2]$ has a birefringence of 0.250 (See Fig. S9a, ESI†), while $Sr_3F_2(VO_2F_4)(IO_3)$ has a birefringence of 0.406 (Fig. 6). These birefringences exceed those of most inorganic oxides (Table S6, ESI†). Moreover, the birefringence of $Sr_3F_2(VO_2F_4)(IO_3)$ is significantly higher than those of all commercially available birefringent crystals and all iodate-fluorides. (See Fig. S9b, ESI†).

Difference between measured and calculated values of birefringence

The birefringence of a crystal is dependent on the direction of the incident light, resulting in a measured value that is typically lower than the calculated value. In the case of biaxial crystals, the crystal exhibits the calculated birefringence value only when the incident light is perpendicular to the plane of the optic axes. The crystal samples of $Sr_3F_2(VO_2F_4)(IO_3)$ used in this study were in their original growth state. The measured birefringence value of the crystal is lower than the calculated value because the plane of incidence is not the plane of the optic axes.
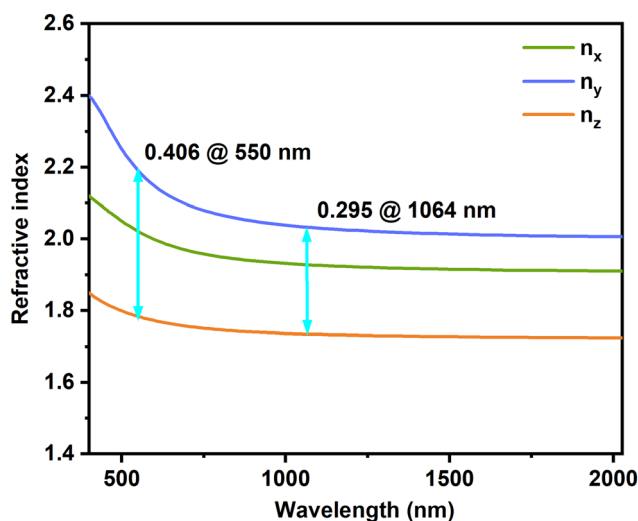

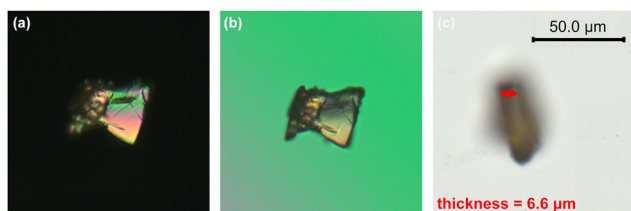**Fig. 5** Original interference image of a single crystal of $Sr_3F_2(VO_2F_4)(IO_3)$ under orthogonally polarized light (a). The crystal under extinction (b). Thickness of the selected measured single crystal (c).

Fig. 6 Calculated frequency-dependent refractive indices of $Sr_3F_2(VO_2F_4)(IO_3)$.

7290 | *J. Mater. Chem. C*, 2024, **12**, 7286–7294

This journal is © The Royal Society of Chemistry 2024

Relationship between crystal structure and birefringence

The correlation between the functional units and birefringence of the materials was analyzed by conducting theoretical calculations of electron density difference. The electron density difference maps show that the anionic functional units are anisotropic, while the electron distribution of the Sr^{2+} cations is spherical. Therefore, the IO_3^- and VO_mF_n functional groups contribute to the significant birefringences of $Sr[VO_2F(IO_3)_2]$ and $Sr_3F_2(VO_2F_4)(IO_3)$ (Fig. 7).

To qualitatively analyze the contribution of the anionic functional units, we calculated the dipole moment vector of each unit. The equation for calculating the dipole moment vector of a molecule is:

$$\vec{\mu} = \sum_i q_i \vec{r_i} \qquad (2)$$

Here, the symbol $\vec{\mu}$ represents the dipole moment vector, q_i denotes the magnitude of the ith charge, and $\vec{r_i}$ represents the position of the ith charge.

For $Sr[VO_2F(IO_3)_2]$, the IO_3^- and VO_4F^{4-} groups have dipole moments of 14.271 D and 0.178 D, respectively (Table S4, ESI†). These values are slightly higher than the dipole moments of the IO_3^- (13.757 D) and VO_4F^{4-} (0.0374 D) groups in the compound α-$Ba[VO_2F(IO_3)_2]$.[38] In $Sr_3F_2(VO_2F_4)(IO_3)$, the IO_3^- and $VO_2F_4^{3-}$ groups have dipole moments of 14.178 D and 9.714 D, respectively (Table S5, ESI†). The dipole moments of these IO_3^- groups are comparable to those of other iodates. The dipole moment of the $VO_2F_4^{3-}$ octahedron (9.714 D) in $Sr_3F_2(VO_2F_4)(IO_3)$ is significantly larger than that of the VO_4F^{4-} polyhedron in $Sr[VO_2F(IO_3)_2]$ (0.178 D) and most d^0-TM polyhedra, such as the VO_5F^{6-} octahedron in $CsVO_2F(IO_3)$ (6.92 D, 0.04 at 2050 nm),[52] the VO_5^{5-} polyhedron in $NaVO_2(IO_3)_2$-(H_2O) (1.94D, 0.15 at 1064 nm),[53] the $VO_4F_2^{5-}$ octahedron and the $VO_3F_2^{3-}$ octahedron in $K_3V_2O_3F_4(IO_3)_3$ (9.10D, 3.92D, 0.158 at 2050 nm),[54] the VO_4^{3-} polyhedron in $Zn_2(VO_4)(IO_3)$ (0.16 D, 0.180 at 1064 nm),[55] the MoO_6^{6-} octahedron in α/β-$BaTeMo_2O_9$ (7.52 D, 6.05 D),[56] and the $ZrO_2F_6^{6-}$ polyhedron in $CsZrF_4(IO_3)$ (0.93 D, 0.20 at 1064 nm).[57] It is evident that non-planar functional groups with large dipole moments contribute to the high birefringence of the material.

Birefringence also depends on the spatial density and arrangement of the functional units. In $Sr[VO_2F(IO_3)_2]$, the

density of IO_3^- is 1.04×10^{-2} Å^{-3}, while in $Sr_3F_2(VO_2F_4)(IO_3)$, the density of IO_3^- plus $VO_2F_4^{3-}$ is smaller, 0.86×10^{-2} Å^{-3}. Therefore, the arrangement of functional units is more important for birefringence. The degree of co-linearity between the units and the angle in relation to the principal refractive axis can be used for evaluation. The smaller the angle, the greater the birefringence. The dipole moment of SCALP IO_3^- is oriented opposite to its lone electron pair. In $Sr[VO_2F(IO_3)_2]$, the angle between the lone pairs of the two IO_3^- groups is $12.06°$, while the angle between the lone electron pairs and the principal axis with the smallest refractive (a axis) is $19.36°$ (Fig. 1b). The two angles in the α-$Ba[VO_2F(IO_3)_2]$ are smaller than those in $Sr[VO_2F(IO_3)_2]$, so the birefringence of α-$Ba[VO_2F(IO_3)_2]$ (0.278 at 550 nm) is larger than that of $Sr[VO_2F(IO_3)_2]$, although the dipole moment of the functional groups of α-$Ba[VO_2F(IO_3)_2]$ is slightly smaller than that of $Sr[VO_2F(IO_3)_2]$. In contrast, the IO_3^- groups in $Sr_3F_2(VO_2F_4)(IO_3)$ have their lone electron pairs arranged in a straight line, with an angle of only $3.0°$ between the lone electron pairs and the crystallographic c axis. Therefore, the IO_3^- groups in $Sr_3F_2(VO_2F_4)(IO_3)$ are much ordered than in $Sr[VO_2F(IO_3)_2]$ and most vanadium–iodates, such as $CsVO_2F(IO_3)$ ($86.8°$, 0.04 at 2050 nm),[52] $Cs_2VOF_4(IO_2F_2)$[58] ($89.9°$, 0.088 at 2050 nm) and α-$Ba_2[VO_2F_2(IO_3)_2]IO_3$ ($30.7°$, $36.2°$ and $33.1°$, 0.20 at 2050 nm),[38] resulting in a greater contributions to the birefringence.

The effect of the arrangement of the SOJT VO_mF_n polyhedron on birefringence becomes more complicated because these units have more than five polarized bonds. It is widely accepted that birefringence is at its maximum when the dipole moment of the polyhedron is parallel to the principal axis with the highest refractive index. In $Sr[VO_2F(IO_3)_2]$, the dipole moments of the VO_4F^{4-} polyhedrons are perpendicular to the principal axis with the highest refractive index, so VO_4F^{4-} units do not contribute to the birefringence of $Sr[VO_2F(IO_3)_2]$.

$Sr_3F_2(VO_2F_4)(IO_3)$ crystallizes in the monoclinic space group. The crystallographic b axis coincides with one of the three refractive principal axes, while the other two are situated in the ac plane at a slight angle to the original orthogonal coordinate axes and the crystallographic axes. The effect of the functional units on birefringence was assessed by measuring the difference between the dipole moment components (ΔM) in the directions of the highest and lowest refractive indices. The results presented in Tables S4 and S5 (ESI†) indicate that $VO_2F_4^{3-}$ contributes to the birefringence, while VO_4F^{4-} does not, with ΔM values of 0 and 1.347 D, respectively.

In summary, by using more fluorine anions to break the V–O–I bonds in the polymerized anions in $Sr[VO_2F(IO_3)_2]$, the discrete IO_3^- groups in $Sr_3F_2(VO_2F_4)(IO_3)$ are optimally aligned, and the anisotropy of the fluorinated $VO_2F_4^{3-}$ polyhedra is much larger than that of the VO_4F^{4-} polyhedra, resulting in a higher birefringence of $Sr_3F_2(VO_2F_4)(IO_3)$.

Fig. 7 Electron density difference maps of $[VO_2F(IO_3)_2]^{2-}$ polyanion (a) and VO_4F^{4-} polyhedron (b) for $Sr[VO_2F(IO_3)_2]$, and IO_3^- group (c) and $VO_2F_4^{3-}$ octahedron (d) for $Sr_3F_2(VO_2F_4)(IO_3)$.

Conclusion

In conclusion, we have successfully synthesized two new VOF polyhedron–iodate, $Sr[VO_2F(IO_3)_2]$ and $Sr_3F_2(VO_2F_4)(IO_3)$. The

This journal is © The Royal Society of Chemistry 2024

J. Mater. Chem. C, 2024, **12**, 7286–7294 | **7291**

two compounds have high birefringence values of 0.250 and 0.406 at 550 nm, as well as wide transmission ranges and high thermal stability, superior to the commercially available birefringent yttrium vanadate (YVO_4), and the compound $Sr_3F_2(VO_2F_4)(IO_3)$ has the largest birefringence in the iodate-fluoride system. The birefringence of $Sr_3F_2(VO_2F_4)(IO_3)$ is 1.6 times higher than that of $Sr[VO_2F(IO_3)_2]$, which is attributed to the fact that the higher concentration of fluorine separates the IO_3^- and $VO_2F_4^{3-}$ functional units and creates a structural template ($Sr_3F_2^{4+}$) that favors the arrangement of the functional groups. The contribution of non-planar functional units to birefringence can be evaluated by qualitatively calculating their dipole moments and the difference in components along the principal axes of the highest and lowest refractive indices. We continue to investigate birefringent materials using functional unit hybridization and structure modulation.

Disclosures

Hydrofluoric acid is a highly corrosive substance that requires careful handling in a fume hood.

Author contributions

Y. Huang synthesized the compounds and performed most experiments. Y. Huang and X. Y. Zhang performed the optical theoretical calculations. S. G. Zhao performed birefringence tests. Y. Huang, B. P. Yang, and J. G. Mao analyzed all the physical tests and wrote the manuscript. All authors provided input on the manuscript.

Conflicts of interest

There is no conflict of interest to report.

Acknowledgements

References

1 Z. Y. Xie, L. G. Sun, G. Z. Han and Z. Z. Gu, Optical Switching of a Birefringent Photonic Crystal, *Adv. Mater.*, 2008, **20**, 3601–3604.

2 X. M. Chen, W. G. Lu, J. L. Tang, Y. Y. Zhang, Y. T. Wang, G. D. Scholes and H. Z. Zhong, Solution-processed inorganic perovskite crystals as achromatic quarter-wave plates, *Nat. Photonics*, 2021, **15**, 813–816.

3 W. Q. Huang, X. Zhang, Y. Q. Li, Y. Zhou, X. Chen, X. Q. Li, F. F. Wu, M. C. Hong, J. H. Luo and S. G. Zhao, A Hybrid Halide Perovskite Birefringent Crystal, *Angew. Chem., Int. Ed.*, 2022, **61**, e202202746.

4 C. Liu, S.-H. Zhou, C. Zhang, Y.-Y. Shen, X.-Y. Liu, H. Lin and Y. Liu, CsCu₃SbS₄: rational design of a two-dimensional layered material with giant birefringence derived from Cu_3SbS_4, *Inorg. Chem. Front.*, 2022, **9**, 478–484.

5 S. Y. Niu, G. Joe, H. Zhao, Y. C. Zhou, T. Orvis, H. Huyan, J. Salman, K. Mahalingam, B. Urwin and J. B. Wu, *et al.*, Giant optical anisotropy in a quasi-one-dimensional crystal, *Nat. Photonics*, 2018, **12**, 392–396.

6 G. Q. Zhou, J. Xu, X. D. Chen, H. Y. Zhong, S. T. Wang, K. Xu, P. Z. Deng and F. X. Gan, Growth and spectrum of a novel birefringent alpha-BaB₂O₄ crystal, *J. Cryst. Grow.*, 1998, **191**, 517–519.

7 G. Ghosh, Dispersion-equation coefficients for the refractive index and birefringence of calcite and quartz crystals, *Opt. Commun.*, 1999, **163**, 95–102.

8 J. R. Devore, Refractive Indices of Rutile and Sphalerite, *J. Opt. Soc. Am.*, 1951, **41**, 416–419.

9 H. T. Luo, T. Tkaczyk, E. L. Dereniak, K. Oka and R. Sampson, High birefringence of the yttrium vanadate crystal in the middle wavelength infrared, *Opt. Lett.*, 2006, **31**, 616–618.

10 D. E. Zelmon, D. L. Small and D. Jundt, Infrared corrected Sellmeier coefficients for congruently grown lithium niobate and 5 mol% magnesium oxide-doped lithium niobate, *J. Opt. Soc. Am. B*, 1997, **14**, 3319–3322.

11 G. D. Boyd, R. C. Miller, K. Nassau, W. L. Bond and A. Savage, LiNbO₃: AN EFFICIENT PHASE MATCHABLE NONLINEAR OPTICAL MATERIAL, *Appl. Phys. Lett.*, 1964, **5**, 234–236.

12 W. B. Zhang, J. B. Huang, S. J. Han, Z. H. Yang and S. L. Pan, Enhancement of Birefringence in Borophosphate Pushing Phase-Matching into the Short-Wavelength Region, *J. Am. Chem. Soc.*, 2022, **144**, 9083–9090.

13 F. Flossmann, U. T. Schwarz, M. Maier and M. R. Dennis, Polarization singularities from unfolding an optical vortex through a birefringent crystal, *Phys. Rev. Lett.*, 2005, **95**, 253901.

14 M. J. Katz, H. Kaluarachchi, R. J. Batchelor, A. A. Bokov, Z. G. Ye and D. B. Leznoff, Highly birefringent materials designed using coordination polymer synthetic methodology, *Angew. Chem., Int. Ed.*, 2007, **46**, 8804–8807.

15 A. Tudi, S. Han, Z. Yang and S. Pan, Potential optical functional crystals with large birefringence: Recent advances and future prospects, *Coord. Chem. Rev.*, 2022, **459**, 214380.

16 X. Meng, W. Yin and M. Xia, Cyanurates consisting of intrinsic planar π-conjugated 6-membered rings: An emerging source of optical functional materials, *Coord. Chem. Rev.*, 2021, **439**, 213916.

17 X. H. Meng, F. Liang, J. Tang, K. J. Kang, W. L. Yin, T. X. Zeng, B. Kang, Z. S. Lin and M. J. Xia, LiO₄ tetrahedra lock the alignment of pi-conjugated layers to maximize optical anisotropy in metal hydroisocyanurates, *Inorg. Chem. Front.*, 2019, **6**, 2850–2854.

18 Z. H. Chen, Z. Z. Zhang, R. L. Wu, X. Y. Dong, Y. J. Shi and Q. Jing, Theoretical study on Pb₂VO₂F₅: large birefringence

7292 | *J. Mater. Chem. C*, 2024, **12**, 7286–7294

This journal is © The Royal Society of Chemistry 2024

derived from optical anisotropies of VO_2F_4 groups, *J. Mater. Sci.*, 2017, **53**, 3483–3492.

19 J.-H. Wu, C.-L. Hu, T.-K. Jiang, J.-G. Mao and F. Kong, Highly Birefringent d0 Transition Metal Fluoroantimonite in the Mid Infrared Band: Order–Disorder Regulation by Cationic Size, *J. Am. Chem. Soc.*, 2023, **145**, 24416–24424.

20 X. Dong, Y. Long, L. Huang, L. Cao, D. Gao, J. Bi and G. Zou, Large optical anisotropy differentiation induced by the anion-directed regulation of structures, *Inorg. Chem. Front.*, 2022, **9**, 6441–6447.

21 J. Guo, J. Huang, A. Tudi, X. Hou, S. Han, Z. Yang and S. Pan, Birefringence Regulation by Clarifying the Relationship Between Stereochemically Active Lone Pairs and Optical Anisotropy in Tin-based Ternary Halides, *Angew. Chem., Int. Ed.*, 2023, **62**, e202304238.

22 S. Liu, X. M. Liu, S. G. Zhao, Y. C. Liu, L. N. Li, Q. R. Ding, Y. Q. Li, Z. S. Lin, J. H. Luo and M. C. Hong, An Exceptional Peroxide Birefringent Material Resulting from d-pi Interactions, *Angew. Chem., Int. Ed.*, 2020, **59**, 9414–9417.

23 C. C. Jin, X. P. Shi, H. Zeng, S. J. Han, Z. Chen, Z. H. Yang, M. Mutailipu and S. L. Pan, Hydroxyfluorooxoborate $Na[B_3O_3F_2(OH)_2][B(OH)_3]$: Optimizing the Optical Anisotropy with Heteroanionic Units for Deep Ultraviolet Birefringent Crystals, *Angew. Chem., Int. Ed.*, 2021, **60**, 20469–20475.

24 Q. Wang, W. Song, Y. Lan, L. L. Cao, L. Huang, D. J. Gao, J. Bi and G. H. Zou, KLi_2CO_3F: a beryllium-free KBBF-type deep-UV carbonate with an enhanced interlayer interaction and large birefringence, *Inorg. Chem. Front.*, 2022, **9**, 3590–3597.

25 W. Xiong, L. Chen, L. X. Huang, F. Y. Guo, Y. Zhou and H. Yuan, Bridgman growth and characterization of birefringent crystal $NaNO_3$, *Cryst. Res. Technol.*, 2015, **50**, 250–254.

26 Y. Li, Ok, K. M. Crystal Growth of $K_2HCO_3F\cdot H_2O$ with a Very Short Cutoff Edge and Large Birefringence, *Cryst. Growth Des.*, 2022, **22**, 5639–5644.

27 J. Y. Guo, A. Tudi, S. J. Han, Z. H. Yang and S. L. Pan, Alpha-SnF_2: A UV Birefringent Material with Large Birefringence and Easy Crystal Growth, *Angew. Chem., Int. Ed.*, 2021, **60**, 3540–3544.

28 Y. Yang, Y. Qiu, P. F. Gong, L. Kang, G. M. Song, X. M. Liu, J. L. Sun and Z. S. Lin, Lone-Pair Enhanced Birefringence in an Alkaline-Earth Metal Tin(II) Phosphate $BaSn_2(PO_4)_2$, *Chem. - Eur. J.*, 2019, **25**, 5648–5651.

29 M. Luo, F. Liang, X. Hao, D. H. Lin, B. X. Li, Z. S. Lin and N. Ye, Rational Design of the Nonlinear Optical Response in a Tin Iodate Fluoride $Sn(IO_3)_2F_2$, *Chem. Mater.*, 2020, **32**, 2615–2620.

30 Y. J. Jia, Y. G. Chen, Y. Guo, X. F. Guan, C. Li, B. Li, M. M. Liu and X. M. Zhang, $LiM(II)(IO_3)_3$ (M(II) =Zn and Cd): Two Promising Nonlinear Optical Crystals Derived from a Tunable Structure Model of alpha-$LiIO_3$, *Angew. Chem., Int. Ed.*, 2019, **58**, 17194–17198.

31 J. Chen, C. L. Hu, F. F. Mao, X. H. Zhang, B. P. Yang and J. G. Mao, $LiMg(IO_3)_3$: An excellent SHG material designed by single-site aliovalent substitution, *Chem. Sci.*, 2019, **10**, 10870–10875.

32 J. Chen, C. L. Hu and J. G. Mao, $LiGaF_2(IO_3)_2$: A mixed-metal gallium iodate-fluoride with large birefringence and wide band gap, *Sci. China Mater.*, 2020, **64**, 400–407.

33 Z. Y. Bai and K. M. Ok, Dramatically improved optical anisotropy by realizing stereochemically active lone pairs in a sulfate system, $K_2SO_4\cdot HIO_3$, *Inorg. Chem. Front.*, 2023, **10**, 1919–1925.

34 C. Wu, X. X. Jiang, Z. J. Wang, L. Lin, Z. S. Lin, Z. P. Huang, X. F. Long, M. G. Humphrey and C. Zhang, Giant Optical Anisotropy in the UV-Transparent 2D Nonlinear Optical Material $Sc(IO_3)_2(NO_3)$, *Angew. Chem., Int. Ed.*, 2020, **133**, 3506–3510.

35 Y. Huang, T. K. Jiang, B. P. Yang, C. L. Hu, Z. Fang and J. G. Mao, Two Indium Iodate–Nitrates with Large Birefringence Induced by Hybrid Anionic Functional Groups and Their Favorable Arrangements, *Inorg. Chem.*, 2022, **61**, 3374–3378.

36 X. H. Zhang, B. P. Yang, J. Chen, C. L. Hu, Z. Fang, Z. Wang and J. G. Mao, A new iodate-phosphate $Pb_2(IO_3)(PO_4)$ achieving great improvement in birefringence activated by $(IO_3)^-$ groups, *Chem. Commun.*, 2020, **56**, 635–638.

37 Y. Huang, Z. Fang, B. P. Yang, X. Y. Zhang and J. G. Mao, A new birefringent material, $HfF_2(IO_3)_2$, with a large birefringence and improved overall performances achieved by the integration of functional groups, *Scr. Mater.*, 2023, **223**, 115082.

38 H. W. Yu, M. L. Nisbet and K. R. Poeppelmeier, Assisting the Effective Design of Polar Iodates with Early Transition-Metal Oxide Fluoride Anions, *J. Am. Chem. Soc.*, 2018, **140**, 8868–8876.

39 R. H. Blessing, An Empirical Correction for Absorption Anisotropy, *Acta Crystallogr., Sect. A: Found. Crystallogr.*, 1995, **51**, 33–38.

40 G. M. Sheldrick, SHELXT - Integrated space-group and crystal-structure determination, *Acta Crystallogr., Sect. A: Found. Adv.*, 2015, **71**, 3–8.

41 A. L. Spek, Single-crystal structure validation with the program PLATON, *J. Appl. Crystallogr.*, 2003, **36**, 7–13.

42 P. Kubelka and F. Munk, The Kubelka-Munk Theory of Reflectance, *Z. Phys. A: Hadrons Nucl.*, 1931, **12**, 593.

43 V. Milman, B. Winkler, J. A. White, C. J. Pickard, M. C. Payne, E. V. Akhmatskaya and R. H. Nobes, Electronic structure, properties, and phase stability of inorganic crystals: A pseudopotential plane-wave study, *Int. J. Quantum Chem.*, 2000, **77**, 895–910.

44 M. D. Segall, P. J. D. Lindan, M. J. Probert, C. J. Pickard, P. J. Hasnip, S. J. Clark and M. C. Payne, First-principles simulation: ideas, illustrations and the CASTEP code, *J. Phys.: Condens. Matter*, 2002, **14**, 2717–2744.

45 J. P. Perdew, K. Burke and M. Ernzerhof, Generalized gradient approximation made simple, *Phys. Rev. Lett.*, 1996, **77**, 3865–3868.

46 Y. L. Hu, X. X. Jiang, C. Wu, Z. P. Huang, Z. S. Lin, M. G. Humphrey and C. Zhang, $A_2MoO_2F_3(IO_2F_2)$ (A = Rb, Cs): Strong Nonlinear Optical Responses and Enlarged Band Gaps through Fluorine Incorporation, *Chem. Mater.*, 2021, **33**, 5700–5708.

This journal is © The Royal Society of Chemistry 2024

J. Mater. Chem. C, 2024, **12**, 7286–7294 | **7293**

47 Q. M. Huang, C. L. Hu, B. P. Yang, Z. Fang, Y. Huang and J. G. Mao, $Ba_2[FeF_4(IO_3)_2]IO_3$: a promising nonlinear optical material achieved by chemical-tailoring-induced structure evolution, *Chem. Commun.*, 2021, **57**, 11525–11528.

48 N. E. Brese and M. Okeeffe, Bond-Valence Parameters for Solids, *Acta Crystallogr., Sect. B: Struct. Sci.*, 1991, **47**, 192–197.

49 D. Altermatt and I. D. Brown, The Automatic Searching for Chemical-Bonds in Inorganic Crystal-Structures, *Acta Crystallogr., Sect. B: Struct. Sci.*, 1985, **41**, 240–244.

50 Q. M. Huang, C. L. Hu, B. P. Yang, R. L. Tang, J. Chen, Z. Fang, B. X. Li and J. G. Mao, $Ba_2[MoO_3(OH)(IO_3)_2]IO_3$: A Promising SHG Material Featuring a Λ-Shaped Functional Motif Achieved by Universal Mono-Site Substitution, *Chem. Mater.*, 2020, **32**, 6780–6787.

51 M. Gajdoš, K. Hummer, G. Kresse, J. Furthmüller and F. Bechstedt, Linear optical properties in the projector-augmented wave methodology, *Phys. Rev. B: Condens. Matter Mater. Phys.*, 2006, **73**, 045112.

52 J. Chen, C. L. Hu, X. H. Zhang, B. X. Li, B. P. Yang and J. G. Mao, $CsVO_2F(IO_3)$: An Excellent SHG Material Featuring an Unprecedented 3D $[VO_2F(IO_3)]^-$ Anionic Framework, *Angew. Chem., Int. Ed.*, 2020, **59**, 5381–5384.

53 B. P. Yang, C. L. Hu, X. Xu, C. F. Sun, J. H. Zhang and J. G. Mao, $NaVO_2(IO_3)_2(H_2O)$: A Unique Layered Material Produces A Very Strong SHG Response, *Chem. Mater.*, 2010, **22**, 1545–1550.

54 J. Chen, C. L. Hu, Y. L. Lin, Y. Chen, Q. Q. Chen and J. G. Mao, $K_3V_2O_3F_4(IO_3)_3$: a high-performance SHG crystal containing both five and six-coordinated V^{5+} cations, *Chem. Sci.*, 2022, **13**, 454–460.

55 B. P. Yang, C. L. Hu, X. Xu, C. Huang and J. G. Mao, $Zn_2(VO_4)(IO_3)$: A Novel Polar Zinc(II) Vanadium(V) Iodate with a Large SHG Response, *Inorg. Chem.*, 2013, **52**, 5378–5384.

56 H. S. Ra, K. M. Ok and P. S. Halasyamani, Combining second-order Jahn-Teller distorted cations to create highly efficient SHG materials: Synthesis, characterization, and NLO properties of $BaTeM_2O_9$ (M = Mo^{6+} or W^{6+}), *J. Am. Chem. Soc.*, 2003, **125**, 7764–7765.

57 L. Lin, X. X. Jiang, C. Wu, Z. S. Lin, Z. P. Huang, M. G. Humphrey and C. Zhang, $CsZrF_4(IO_3)$: The First Polar Zirconium Iodate with *cis*-$[ZrO_2F_6]$ Polyhedra Inducing Optimized Balance of Large Band Gap and Second Harmonic Generation, *Chem. Mater.*, 2021, **33**, 5555–5562.

58 M. M. Ding, H. P. Wu, Z. G. Hu, J. Y. Wang, Y. C. Wu and H. W. Yu, $Cs_2VOF_4(IO_2F_2)$: Rationally designing a noncentrosymmetric early-transition-metal fluoroiodate, *J. Mater. Chem. C*, 2022, **10**, 12197–12201.

7294 | *J. Mater. Chem. C*, 2024, **12**, 7286–7294

This journal is © The Royal Society of Chemistry 2024